



1 Coupling the ParFlow Integrated Hydrology Model within the NASA Land 2 Information System: A case study over the Upper Colorado River Basin

3
4 ^{1,4,7}Peyman Abbaszadeh, ³Fadji Zaoua Maina, ^{1,4}Chen Yang, ⁵Dan Rosen, ³Sujay Kumar,
5 ⁶Matthew Rodell, ^{1,2,4}Reed Maxwell

6
7 ¹Department of Civil and Environmental Engineering, Princeton University, Princeton, NJ, USA

8 ²High Meadows Environmental Institute, Princeton University, Princeton, NJ, USA

9 ³Hydrological Sciences Laboratory, NASA Goddard Space Flight Center, Greenbelt, MD, USA

10 ⁴Integrated GroundWater Modeling Center, Princeton University, Princeton, NJ USA

11 ⁵Climate & Global Dynamics Lab, The National Center for Atmospheric Research, Boulder,
12 Colorado, USA

13 ⁶ Earth Sciences Division, NASA Goddard Space Flight Center, Greenbelt, MD, USA

14 now at ⁷Department of Civil and Environmental Engineering, Hydrologic Modeling and
15 Assimilation Lab, Portland State University, Portland, OR

16 Corresponding author: Peyman Abbaszadeh, pabbaszadeh@princeton.edu,
17 pabbaszadeh@pdx.edu
18

19 Abstract

20 Understanding, observing, and simulating Earth's water cycle is imperative for effective water
21 resource management in the face of a changing climate. NASA's Land Information System
22 (LIS)/Noah-MP and the ParFlow groundwater model are the two widely used modeling platforms
23 that enable studying the Earth's land surface and subsurface hydrologic processes, respectively.
24 The integration of ParFlow and LIS/Noah-MP models and harnessing their strengths can provide
25 an opportunity to simulate surface terrestrial water processes and groundwater dynamics together
26 while enhancing the accuracy and scalability of hydrological modeling. This study introduces
27 ParFlow-LIS/Noah-MP (PF-LIS/Noah-MP), which is an integrated, physically based hydrologic
28 modeling framework. PF-LIS/Noah-MP enables the user to simulate land surface processes in
29 conjunction with subsurface hydrologic processes while considering the interactions between the
30 two. In this study, we compared the results of the coupled PF-LIS/Noah-MP and standalone
31 LIS/Noah-MP models with a suite of in-situ and satellite observations over the Upper Colorado
32 River Basin (UCRB) in the United States. This analysis confirmed that integrating ParFlow with
33 LIS/Noah-MP not only enhances the capability of LIS/Noah-MP in estimating land surface
34 processes over regions with complex topography but also enables it to accurately simulate
35 subsurface hydrologic processes.

36 Keywords: ParFlow, LIS/Noah-MP, PF-LIS/Noah-MP, hydrology model, groundwater



37 1. Introduction

38 The interaction of surface and subsurface hydrologic processes is complex and dynamic.
39 Surface hydrologic processes include the movements of water on the land surface, such as runoff,
40 while subsurface hydrologic processes include the movements of water below the ground, such as
41 infiltration and groundwater flow. These surface and subsurface physical processes are
42 interconnected through various mechanisms. For instance, precipitation that falls on the land
43 surface can infiltrate the soil and become soil moisture or runoff into nearby streams and rivers.
44 Soil moisture can either return to the atmosphere through evapotranspiration or percolate into the
45 subsurface, replenishing groundwater storage. Streams and rivers can also recharge underlying
46 groundwater aquifers, and groundwater can discharge into rivers and streams (Fleckenstein et al.,
47 2010; Kalbus et al., 2006; Kourakos et al., 2019; Ntona et al., 2022; Winter et al., 1998).

48 The interaction of surface and subsurface hydrologic processes is particularly relevant to
49 managing water resources in arid and semi-arid regions, where water resources are often limited
50 (Deb et al., 2019; Scanlon et al., 2012; Tian et al., 2015; Wada et al., 2010). Climate change can
51 impact surface and subsurface hydrologic processes and their interactions and feedback to the
52 atmosphere. In particular, changes in precipitation patterns, temperature, and evapotranspiration
53 rates can affect the balance and feedback between surface water and groundwater, affecting water
54 availability and quality (Alley, 2007; Christensen et al., 2004; Oki and Kanae, 2006; Scanlon et
55 al., 2012). Besides, human activities, such as irrigation and water pumping, can alter the natural
56 behavior of surface–subsurface interactions (Boucher et al., 2004; Gordon et al., 2005; Leng et al.,
57 2014; Leung et al., 2011; Liang et al., 2003; Sacks et al., 2009; Tang et al., 2007; Tian et al., 2015),
58 affect the land-atmosphere coupling (Harding and Snyder, 2012; Kawase et al., 2008; Lo and
59 Famiglietti, 2013; Qian et al., 2013) and compromise the health of ecosystems and water quality
60 (Green et al., 2011; Jasechko et al., 2017; Scanlon et al., 2012).

61 Irrigation water use in the Upper Colorado River Basin (UCRB) is a substantial and
62 growing demand on the region's limited water resources. UCRB includes parts of Colorado,
63 Wyoming, Utah, and New Mexico and is home to a large agricultural sector. The region's irrigated
64 agriculture mostly relies on groundwater (Hutson et al., 2004; Kenny et al., 2005). Studies show
65 that due to the recent prolonged drought across the western US (Cook et al., 2015, 2021; Williams
66 et al., 2022), water managers have increased their dependence on groundwater to secure public
67 water supply and irrigate agricultural lands (Famiglietti et al., 2011, 2013; Taylor et al., 2013).



68 Groundwater pumping is an important source of water for agriculture in the UCRB, particularly
69 when and where surface water availability is limited (Castle et al., 2014). Excessive pumping can
70 lead to the depletion of aquifers, impacting water availability and the long-term sustainability of
71 agricultural practices. To address these challenges, many states in the UCRB have implemented
72 regulations and policies to manage groundwater use in agriculture, such as implementing
73 groundwater monitoring programs and setting limits on the amount of water that can be pumped
74 (Supplemental Environmental Impact Statement for Near-term Colorado River Operations; U.S.
75 Department of the Interior, 2021). In general, water management strategies can benefit from
76 skillful hydrologic modeling that considers the land surface and subsurface physical processes in
77 a coupled fashion. In this work, we introduce and test a coupled land surface-subsurface hydrology
78 model (hereafter integrated hydrologic model) as one means to address this need.

79 Integrated hydrologic models have been highly successful in a broad range of watershed-
80 scale studies (see Table 1 in Maxwell et al., 2014). These models represent observed surface and
81 subsurface behavior, diagnose stream–aquifer and land–energy interactions, and enhance our
82 understanding of how disturbances like changes in land-cover and human-induced climate change
83 affect different layers of the hydrologic system (Maxwell et al., 2015). The importance of the
84 interactions between groundwater and surface water and the use of integrated hydrologic models
85 to better understand this connection has been the subject of many studies in the past decade
86 (Barthel and Banzhaf, 2016; Brookfield et al., 2023; Kuffour et al., 2020; Lahmers et al., 2022;
87 O’neill et al., 2021a; Wang and Chen, 2021; Yang et al., 2021). Until recently, integrated
88 hydrologic models were mainly used at local to regional scales, as their implementation required
89 extensive computational resources. However, recent advances in parallel High-Performance
90 Computing (HPC) techniques, numerical solvers, and observational data have made it feasible to
91 conduct large scale, high-resolution simulations of the terrestrial hydrologic cycle (Kollet et al.,
92 2010; Maxwell, 2013; Maxwell et al., 2015; Naz et al., 2023). This has opened up new possibilities
93 for the practical application of integrated hydrologic models at regional to continental scales. Most
94 previous large-scale subsurface studies have not accounted for surface processes explicitly (Fan et
95 al., 2007, 2013; Miguez-Macho et al., 2007). Similarly, many continental to global-scale surface
96 hydrology studies have ignored groundwater or used a highly simplified model, despite the
97 importance of lateral groundwater flows (Krakauer et al., 2014). This limitation has been observed
98 in studies such as those conducted by Döll et al. (2012), Maurer et al. (n.d.), and Xia et al. (2012).



99 The NASA Land Information System (LIS) is a software framework designed to facilitate
100 the integration of land surface models and satellite remote sensing data for improved understanding
101 and prediction of land surface processes (Kumar et al., 2006, 2008a; Peters-Lidard et al., 2007).
102 LIS has been widely used for a variety of scientific and practical applications, including drought
103 monitoring and prediction, water resource management, and flood forecasting, among others
104 (Crow et al., 2012; Getirana et al., 2020; Li et al., 2019; Mocko et al., 2021; Nie et al., 2022). LIS
105 has been integrated with other Earth system modeling systems. For example, a coupled high
106 resolution land-atmosphere system has been developed by coupling LIS with the Weather
107 Research and Forecasting (WRF) model (Kumar et al., 2008a). This coupled land-atmosphere
108 system facilitates study of the interactions between the atmosphere and land surface processes.

109 ParFlow is a robust and versatile groundwater model that integrates advanced numerical
110 techniques to simulate both saturated and unsaturated flow conditions. This model has been
111 coupled with different land surface and atmospheric models to better understand the interactions
112 between the subsurface, surface, and atmospheric processes (Kollet and Maxwell, 2006; Maxwell
113 et al., 2007, 2011, 2014b). Herein, we introduce a newly developed coupled land surface and
114 subsurface hydrology model, ParFlow-LIS/Noah-MP (PF-LIS/Noah-MP) and study its
115 effectiveness and usefulness for simulating land surface and subsurface hydrologic processes. We
116 encourage the readers to refer to Fadji et al (2024) for more information about the coupled system.
117 This paper has been under review at the time of writing this manuscript. Our primary objective is
118 to study the degree to which the coupled PF-LIS/Noah-MP model (Fadji et al 2024) can contribute
119 to better representation of surface and subsurface processes over UCRB. In particular, we study
120 the extent to which the land surface water flux estimates in the LIS/Noah-MP model are improved
121 by coupling it with the ParFlow groundwater model. For this purpose, we compared the coupled
122 PF-LIS/Noah-MP and LIS/Noah-MP model estimates of soil moisture, streamflow, water table
123 depth and terrestrial water storage with a suite of in-situ and satellite observations over the UCRB
124 in the United States.

125 The paper is organized as follows: first, we briefly describe the ParFlow and LIS/Noah-
126 MP model. Next, we discuss the coupling framework. In the results and discussion section of the
127 paper, we provide a comparison of the model simulations against observations and explore how
128 the coupled system could improve understanding of the land surface processes.

129



130 2. ParFlow

131 ParFlow (PARallel Flow) (Ashby and Falgout, 1996; Jones and Woodward, 2001; Kollet
132 and Maxwell, 2006) is an integrated, parallel model platform that simultaneously solves variably
133 saturated three-dimensional Richards' equation throughout the entire subsurface (Kollet and
134 Maxwell, 2008). ParFlow does not separate the phreatic and vadose zones, it employs a unified
135 solution by solving the compressible Richards' equation everywhere in the subsurface. This
136 inclusive methodology allows to obtain a realistic representation of groundwater dynamics, shaped
137 by the underlying geology and topography. In addition to its capability to simulate subsurface
138 flow, ParFlow also tackles the complexities of overland flow and surface runoff. This is
139 accomplished through a combination of continuity or Manning's equations, implemented in either
140 kinematic or diffusive formats. By integrating these surface water flow components, ParFlow
141 offers a fully integrated system that simultaneously solves the partial differential equations (PDEs)
142 governing both surface water and subsurface flow (e.g. Kollet and Maxwell, 2006). Importantly,
143 this integration is achieved in a globally implicit manner, ensuring the robust and efficient solution
144 of these interconnected processes at each time step. The terrain following grid formulation in
145 ParFlow is important for accurately representing topography (Maxwell, 2013). By solving the
146 three-dimensional Richards' equation for variably saturated groundwater flow, the model
147 simulates lateral groundwater flow and replicates the spatial and temporal variations of the water
148 table. It is important to note that groundwater may take a longer time (for example compared to
149 soil moisture) to reach a steady-state due to such a complicated subsurface configuration, which
150 makes it a computationally intensive problem to solve (Maxwell et al., 2014a).

151 3. LIS

152 Since the LIS framework has already been extensively described in the original papers
153 (Kumar et al., 2006; Peters-Lidard et al., 2007), here we only briefly review its main components
154 and features. Land surface modeling within LIS relies on three key inputs: (1) initial conditions,
155 describing the land surface's starting state; (2) boundary conditions, encompassing the atmospheric
156 fluxes or 'forcings' (upper boundary condition) and soil fluxes or states (lower boundary
157 condition); and (3) parameters, which represent the soil, vegetation, topography, and other land
158 surface characteristics. Using these inputs, Land Surface Models (LSMs) available within LIS
159 (e.g., Community Land Model (CLM), Noah-MP, Variable Infiltration Capacity (VIC), Mosaic



160 and Hydrology with Simple SIB (HySSIB)) solve the governing equations of the soil-vegetation-
161 snowpack medium, and estimate the surface fluxes (i.e., sensible and latent heat, ground heat,
162 surface and subsurface runoff, and evapotranspiration) and states (i.e., soil moisture and
163 temperature, snow water equivalent and depth). One of the significant features of LIS is its high-
164 performance land surface modeling and Data Assimilation (DA) infrastructure (Kumar et al.,
165 2008b). Its DA capability enables users to utilize a wide range of in-situ and satellite observations,
166 integrating them into various land surface models (those mentioned above) to enhance their
167 predictive skill while accounting for the different sources of uncertainty involved in different
168 layers of simulation. The DA embedded within LIS provides a possibility to perform probabilistic
169 simulations, which facilitate uncertainty characterization/quantification and help risk assessment
170 and effective decision making in the case of studying extreme hydrologic processes, such as floods
171 and droughts, among others.

172 In this study, we used the Noah-MP LSM (Niu et al., 2011) within LIS (LIS/Noah-MP).
173 In LIS/Noah-MP, groundwater storage changes are represented using a simplified bucket-type
174 linear reservoir approach. This method tracks variations in groundwater storage based on inflow,
175 known as recharge, and outflows, which include capillary rise and base flow. It is important to
176 note that this approach does not explicitly consider complex hydraulic properties such as hydraulic
177 conductivity, a parameter typically used in soil moisture modeling and, by extension, groundwater
178 recharge prediction (Li et al., 2021).

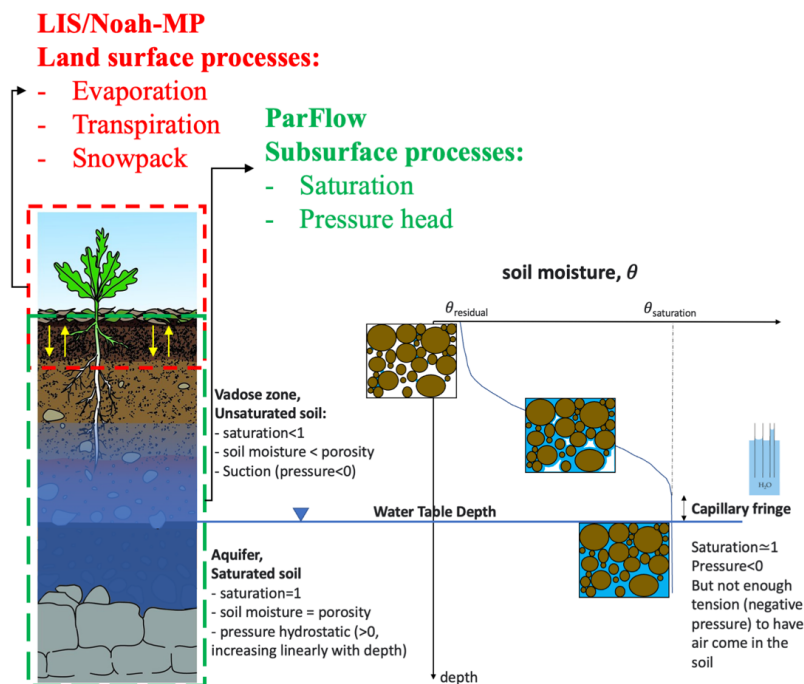
179

180 **4. ParFlow-LIS**

181 Here we describe how we coupled the ParFlow and LIS models. As we mentioned earlier,
182 in the coupled system (PF-LIS/Noah-MP), when the precipitation reaches the ground and
183 infiltrates the soil, LIS estimates the land surface processes (such as evaporation and transpiration)
184 and then calculates the net downward water flux which is later used as input to feed the ParFlow
185 model. It should be noted that the land surface model (LIS/Noah-MP) and groundwater model
186 (ParFlow) share the top four soil layers as the coupled soil zone where the two systems
187 communicate. ParFlow utilizes the Richards' equation to estimate the soil moisture in the coupled
188 zone and in the other soil layers down to the bottom layer. In the PF-LIS/Noah-MP system, in
189 addition to the top four soil layers with depth ranges from 0-0.1m, 0.1-0.4m, 0.4-1m, and 1-2m,
190 there are six additional layers, each with varying soil depths, ranging from 2-7m, 7-17m, 17-42m,



191 42-92m, 92-192m, to the bottom layer from 192-492m. By using saturation data generated by
192 ParFlow as one of its outputs and incorporating the soil layer porosity values, the LIS/Noah-MP
193 model calculates the soil moisture content (θ). This 3D moisture data, derived from ParFlow,
194 replaces the 1D soil hydrology within the LIS/Noah-MP model, affecting the simulation of other
195 land surface processes by LIS/Noah-MP. This is a two-way coupling; at each time step, LIS/Noah-
196 MP computes evaporation, transpiration, snowmelt, and throughfall and passes these to ParFlow
197 and then ParFlow feeds back a new soil moisture field to LIS/Noah-MP. Figure 1 schematically
198 illustrates the soil column, with red and green boxes delineating the control volumes for LIS/Noah-
199 MP and ParFlow, respectively. Where these two areas overlap (shown with yellow arrow) is the
200 coupled soil zone (top four soil layers). The initial soil moisture condition starts from the land
201 surface with θ_{residual} (θ can be any value depending on condition) and varies down to the water
202 table depth, where the soil becomes saturated ($\theta_{\text{saturation}}$). Above the water table, the pressure
203 head is negative, while below the water table in the saturated soil zone, it becomes positive.
204 ParFlow provides estimates of pressure head and soil saturation, which, along with soil-specific
205 storage and porosity, are used to calculate subsurface storage. Through ParFlow, we can estimate
206 groundwater storage and lateral flow, both of which significantly impact the land surface energy
207 and water flux estimates within the land surface model. By integrating ParFlow with LIS/Noah-
208 MP, we can accurately estimate the groundwater storage and account for subsurface lateral flow,
209 facilitating the communication between the land surface and subsurface hydrologic processes.
210



211
 212
 213
 214
 215
 216

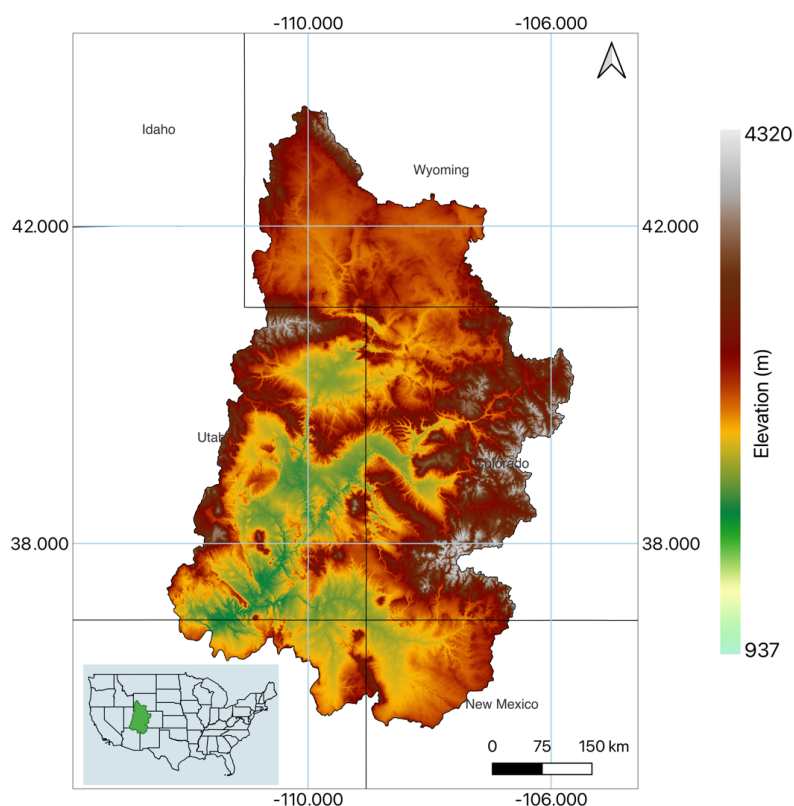
Figure 1. Schematic of the coupled PF-LIS/Noah-MP model. Single soil column representing the coupling zone between the LIS/Noah-MP and ParFlow.

217 5. Study Area

218 This study is conducted over the UCRB, a snow-dominated region covering approximately
 219 280,000 km². Stretching from the river's origins in the Rocky Mountains of Colorado and
 220 Wyoming to its endpoint at Lee's Ferry in Northern Arizona, the basin exhibits a significant
 221 variation in elevation, ranging from 4,320 meters to 937 meters (Figure 2). Throughout the winter
 222 season, which encompasses the period from October through the end of April, the snow covered
 223 area within the UCRB fluctuates between 50,000 km² and 280,000 km². This seasonal change in
 224 snow covered area plays a pivotal role in both the energy dynamics and hydrological cycle of the
 225 region (Liu et al., 2015; Painter et al., 2012). The Colorado River is the primary water source for
 226 over 35 million people in the United States and an additional 3 million in Mexico. A recent
 227 publication by the US Geological Survey (Miller et al., 2016) indicates that up to half of the water
 228 coursing through the rivers and streams within the Upper Colorado River Basin originates from



229 groundwater sources. Recognizing the extent of available groundwater and understanding its
230 replenishment process holds significant importance for the sustainable management of both
231 groundwater and surface water resources within the Colorado River basin. For more information
232 about UCRB, its climatology and geology etc., we refer interested readers to Miller et al (2016).
233



234

235 *Figure 2. Topography of the Upper Colorado River Basin (UCRB) and its location in the US.*

236

237 **6. In-situ Observations and Satellite Products**

238 In this section we describe all those in-situ observations and satellite products that are used
239 for validation of model simulations. As for in-situ observations, we use soil moisture datasets
240 available from multiple observation networks over UCRB, USGS streamflow stations and
241 groundwater monitoring wells. The locations of these in-situ stations are shown in Figure 3. To
242 employ the maximum number of soil moisture stations covering the region, we used datasets
243 provided by ISMN (International Soil Moisture Network) which collected and compiled multiple

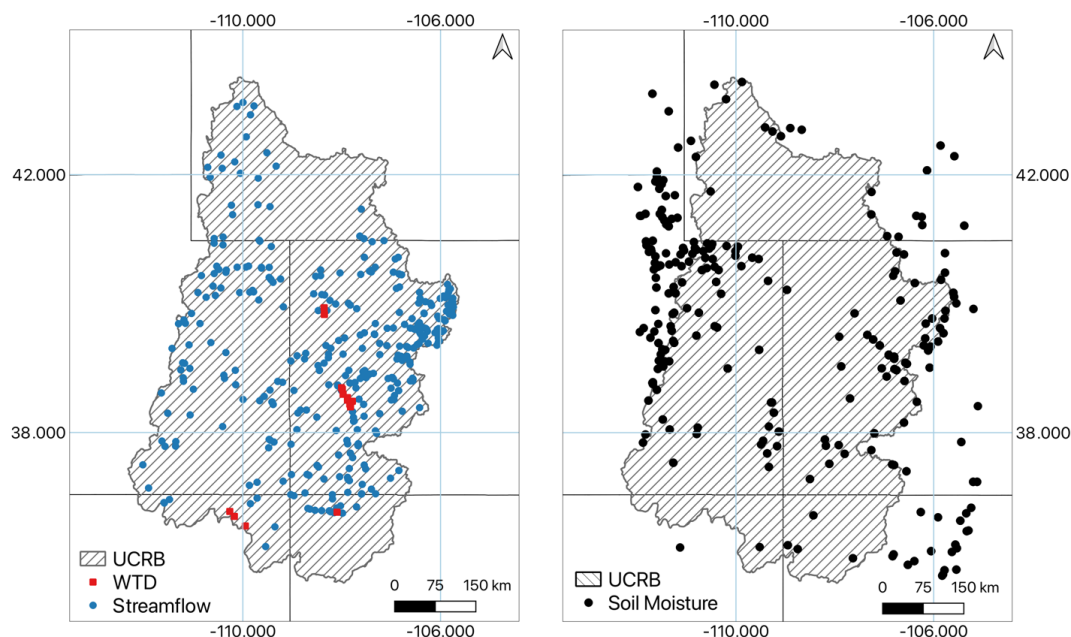


244 networks including, ARM (Atmospheric Radiation Measurement), PBO_H2O (Plate Boundary
245 Observatory), SCAN (Soil Climate Analysis Network), SNOTEL (SNOW TELEmetry), USCRN
246 (U.S. Climate Reference Network), and iRON (Roaring Fork Observation Network). In total, we
247 have data from 238 soil moisture stations in the UCRB and its vicinity (see Figure 3). The
248 distribution of these stations by soil depth is as follows: Layer #1 (0-0.1 meters): 235 stations,
249 Layer #2 (0.1-0.4 meters): 218 stations, Layer #3 (0.4-1 meter): 216 stations, Layer #4 (1-2
250 meters): 41 stations. Having data from multiple depths improves the comparison with simulated
251 soil moisture and hence the evaluation of the coupled PF-LIS system. The soil moisture datasets
252 are publicly available at <https://ismn.earth/en/>. Streamflow and water table depth data are available
253 at <https://waterdata.usgs.gov/nwis/rt> and <https://waterdata.usgs.gov/nwis/gw>, respectively. We
254 made use of data from the period 2002 to 2022. In total, there are 374 USGS stream stations and
255 18 USGS groundwater monitoring wells in the UCRB with observations from 2002 to 2022.
256 Measurements failing to meet the USGS quality control criteria (e.g., those flagged for potential
257 measurement inconsistency or negative outlier values) were removed.

258 In addition, we used two satellite products to investigate the effectiveness of PF-LIS/Noah-
259 MP in estimating the soil moisture and terrestrial water storage. For soil moisture, we use THySM
260 (Thermal Hydraulic disaggregation of Soil Moisture; Liu et al (2022)). This is a downscaled
261 version of SMAP (Soil Moisture Active Passive) satellite soil moisture data, which has 1-km
262 spatial resolution and is available on a daily time scale. THySM shows higher accuracy than the
263 SMAP / Sentinel-1 (SPL2SMAP_S) 1 km SM product when compared to in situ measurements.
264 Anomalies of Terrestrial Water Storage (TWS), derived from Gravity Recovery and Climate
265 Experiment (GRACE; Tapley et al., 2004) and GRACE Follow On (GRACE-FO; Landerer et al.,
266 2020) satellite observations, were compared to those from the coupled PF-LIS system. Launched
267 in 2002 and 2018, GRACE and GRACE-FO have provided monthly, global maps of fluctuations
268 in terrestrial water storage (i.e., the sum of groundwater, soil moisture, surface waters, snow and
269 ice), based on precise monitoring of variations in Earth's gravity field via its effects on the orbits
270 of a pair of twin satellites (http://www2.csr.utexas.edu/grace/RL05_mascons.html). The dataset
271 employed in this study, known as CSR Release-06 GRACE Mascon Solutions, was disseminated
272 by the Center for Space Research (CSR) at the University of Texas, Austin (Save et al., 2016). A
273 monthly TWS anomaly represents the current value minus the 2004 to 2010 mean. While GRACE
274 can detect TWS anomalies relative to the long term mean, it cannot quantify the absolute water



275 mass stored. Due to its relatively coarse spatial resolution ($> 100,000 \text{ km}^2$) it has primarily been
276 used to study major river basins and other large regions (Rodell and Reager, 2023; Scanlon et al.,
277 2016). UCRB with approximately $280,000 \text{ km}^2$ area meets this criterion.
278



279
280
281
282

Figure 3. Location of in-situ soil moisture, USGS streamflow, and WTD stations.

283 7. PF-LIS/Noah-MP Model Setup

284 7.1. Input Datasets

285
286 In this study, we classified model parameters into two categories: surface and subsurface
287 characteristics. The surface parameters, which encompass topographic slopes and land cover data,
288 were determined as follows: Topographic slopes were calculated using the Priority Flow toolbox
289 (Condon and Maxwell, 2019), employing elevation data from the hydrological data and maps
290 derived from Shuttle Elevation Derivatives at multiple Scales (HydroSHEDS) as detailed and
291 tested in Zhang et al (2021). Land cover information was extracted from the National Land Cover
292 Database (NLCD) at a 30-meter resolution and subsequently rescaled to match the model's 1-
293 kilometer resolution (see Figure S1 in the supplementary file). The land cover values are based on



294 the classifications of the International Geosphere-Biosphere Program (IGBP). Regarding the
295 subsurface components of the ParFlow domain, they consist of four soil layers at the top (with
296 depths of 0.1, 0.3, 0.6, and 1 m, starting from the surface and totaling 2 m) and six geology layers
297 at the bottom (with depths of 5, 10, 25, 50, 100, and 200 m, starting from the surface and totaling
298 390 m). The development of the 3D subsurface, which includes soil, unconsolidated, a semi-
299 confining layer, bedrock aquifers, and the 3D model grid, is detailed in Tijerina-Kreuzer et al
300 (2024). The subsurface parameters (e.g. saturated hydraulic conductivity, porosity, and van
301 Genuchten parameters for the soil and subsurface) are detailed in Tijerina-Kreuzer et al (2024) and
302 Yang et al (2023). For the atmospheric forcing data, we use the phase-2 of the North American
303 Land Data Assimilation System (NLDAS-2) product (<https://ldas.gsfc.nasa.gov/nldas/v2/forcing>).
304 This dataset has eight variables: precipitation, air temperature, short-wave and long-wave
305 radiation, wind speed in two directions (east-west and south-north), atmospheric pressure, and
306 specific humidity.

307
308

309 **7.2. Model Spinup**

310

311 To be able to spinup the PF-LIS/Noah-MP model, we need to first spinup ParFlow and
312 LIS/Noah-MP individually and make sure both systems have the most realistic initial conditions.
313 The initial condition (i.e., pressure head) for the ParFlow model was directly obtained from Yang
314 et al (2023). who spunup the ParFlow model over the entire CONUS. We subsetted the UCRB
315 region from that initial pressure file. For more information about the ParFlow spinup process etc.
316 we refer the interested readers to Yang et al (2023). To spin up the LIS/Noah-MP model over
317 UCRB, we ran LIS/Noah-MP over 20 years (from 2002 to 2022) three times. To run the LIS/Noah-
318 MP model, we use the NASA Land surface Data Toolkit (Arsenault et al., 2018), to create the
319 LIS/Noah-MP domain file that encompasses all the parameters that LIS/Noah-MP requires to run.
320 Next, we use the initial conditions for both ParFlow and LIS/Noah-MP, to perform the PF-
321 LIS/Noah-MP model spinup. We ran the PF-LIS/Noah-MP over the period of water year 2005 (a
322 normal water year, not dry and not wet) six times, which was sufficient to bring the PF-LIS/Noah-
323 MP system into quasi-equilibrium.



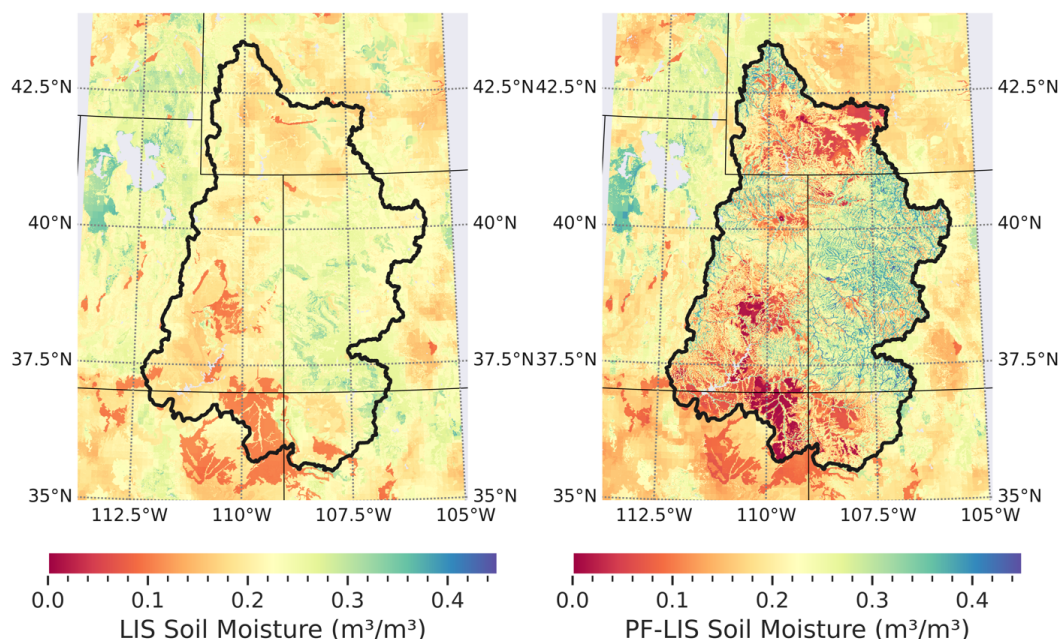
324 **8. Results and Discussion**

325 In this section, we discuss the results of the PF-LIS/Noah-MP model simulations and aim to
326 gain a comprehensive understanding of how the coupled system can enhance the modeling of land
327 surface processes and provide an accurate representation of groundwater storage. Using the initial
328 conditions derived from the model's spinup process, we ran the PF-LIS/Noah-MP model over a
329 20-year period, spanning from 2002 to 2022. Concurrently, we ran the LIS/Noah-MP model for
330 the same time frame, facilitating a comparative analysis of the two model outputs. All model setup
331 and simulations were executed on the NASA Discover High-Performance Computing (HPC)
332 cluster. On average, a one-year simulation utilized approximately 295,000 core hours, resulting in
333 roughly one day of wall-clock time. The entire 20-year simulation consumed approximately 6
334 million core hours of computing time, extending over approximately 1.5 months of wall-clock
335 time.

336

337 **8.1. Soil Moisture Analysis**

338 Here, we study the extent to which the coupled system contributes to an improved
339 representation of soil moisture in the top four soil layers (referred to as the coupling soil zone),
340 where the two models interact. Figure 4 illustrates the topsoil moisture (with ~10 cm depth) as
341 simulated by the LIS/Noah-MP model (left panel) and the PF-LIS/Noah-MP model (right panel).
342 Note that the PF-LIS/Noah-MP simulations are limited to the UCRB region, which accounts for
343 the similarity in model results beyond the boundaries of this region. The results indicate that the
344 soil moisture output from the LIS/Noah-MP model generally aligns with the patterns of soil texture
345 and land cover. However, the soil moisture data generated by the PF-LIS/Noah-MP model
346 represents soil moisture distribution in a manner that closely correlates with topographical and
347 land surface characteristics. In a broad sense, both models demonstrate wet conditions across the
348 eastern UCRB and drier conditions towards the western regions. PF-LIS/Noah-MP provides soil
349 moisture data with higher spatial representativeness, which can be crucial for many applications.
350 For example, such finer spatial representations can be useful irrigation management applications,
351 which allows farmers to make better decisions about when and how much to irrigate, leading to
352 efficient water use and potentially higher crop yields.



353

354 *Figure 4. Spatial pattern of topsoil layer moisture estimated by LIS/Noah-MP (left panel) and*
355 *PF-LIS/Noah-MP (right panel). This result is reported for 01/23/2002.*

356

357

358

359

360

361

362

363

364

365

366

367

368

369

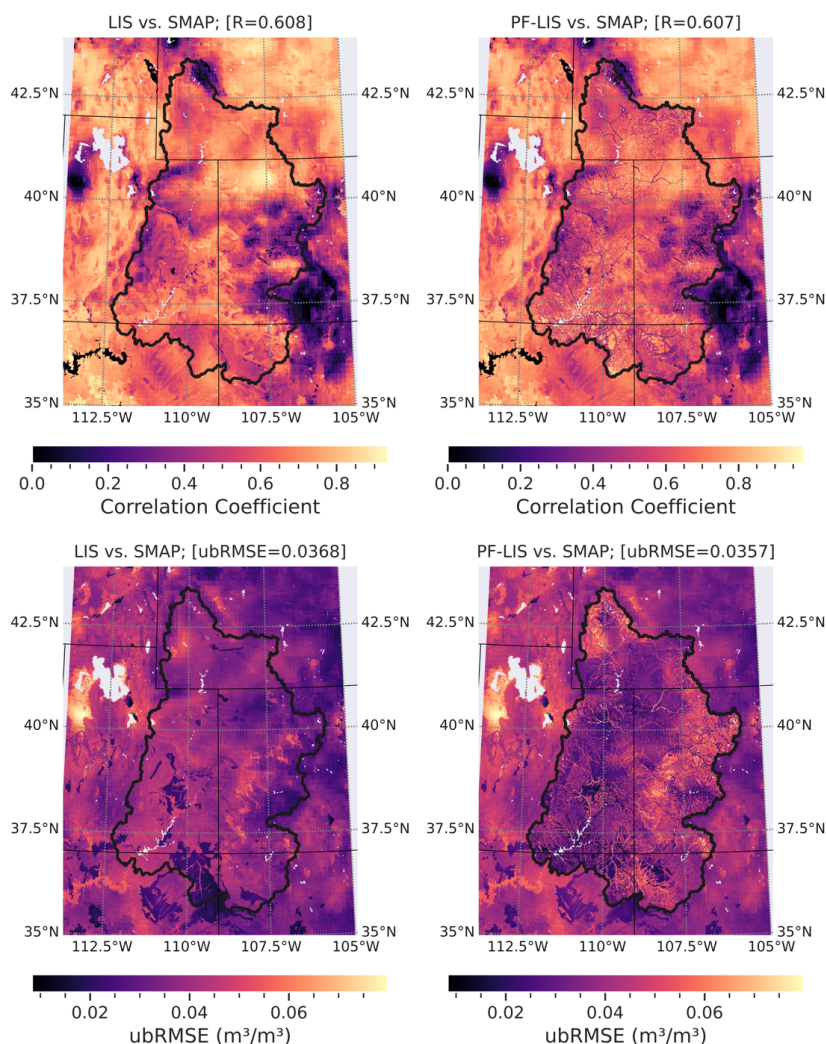
370

371

To further study the model simulation results, we conducted a comparative analysis between PF-LIS/Noah-MP and LIS/Noah-MP-estimated soil moisture values and the satellite-based soil moisture product obtained from SMAP. As previously noted, our analysis employed downscaled soil moisture data with a spatial resolution of 1 kilometer, which is consistent with the resolution of the model simulation, thereby enhancing the accuracy of our comparative analysis. Figure 5 illustrates the outcomes, with the first row depicting the correlation coefficients and the second row showing the unbiased root mean square error (ubRMSE). The ubRMSE serves as a metric that SMAP utilizes for reporting product accuracy. The SMAP mission requirement for soil moisture product accuracy sets the ubRMSE at $0.040 \text{ m}^3/\text{m}^3$ (Chan et al., 2016). Due to the temporal coverage of the SMAP satellite, we calculated both performance metrics over the period of April 2015 to December 2022. To perform this, we used the NASA Land surface Verification Toolkit (LVT; Kumar et al. 2012), which enables rapid evaluation of model simulations by comparing against a comprehensive suite of in-situ, remote sensing, and model and reanalysis data products (<https://lis.gsfc.nasa.gov>). As shown in Figure 5, in general, both performance measures from both models show a similar spatial pattern across the UCRB. Further analysis revealed that,



372 particularly in regions characterized by higher altitudes and complex topography, PF-LIS/Noah-
373 MP-derived soil moisture values closely follow the SMAP observations, outperforming the
374 performance of LIS/Noah-MP-derived soil moisture.



375
376
377
378

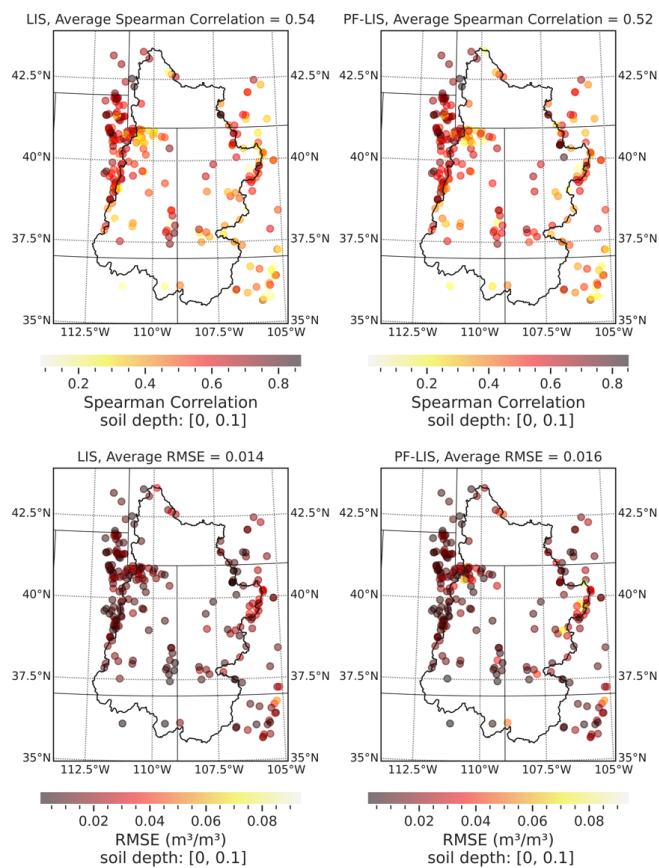
Figure 5. The correlation coefficient and ubRMSE between the simulated topsoil moisture and the SMAP product at 1-km spatial resolution. This result is reported for the period of April 2015 to December 2022.

379 The results also reveal that, in general, when we coupled ParFlow with LIS/Noah-MP, it
380 resulted in soil moisture fields with more spatial detail while keeping the accuracy in the same
381 range as compared to the LIS/Noah-MP standalone soil moisture estimates. ParFlow and



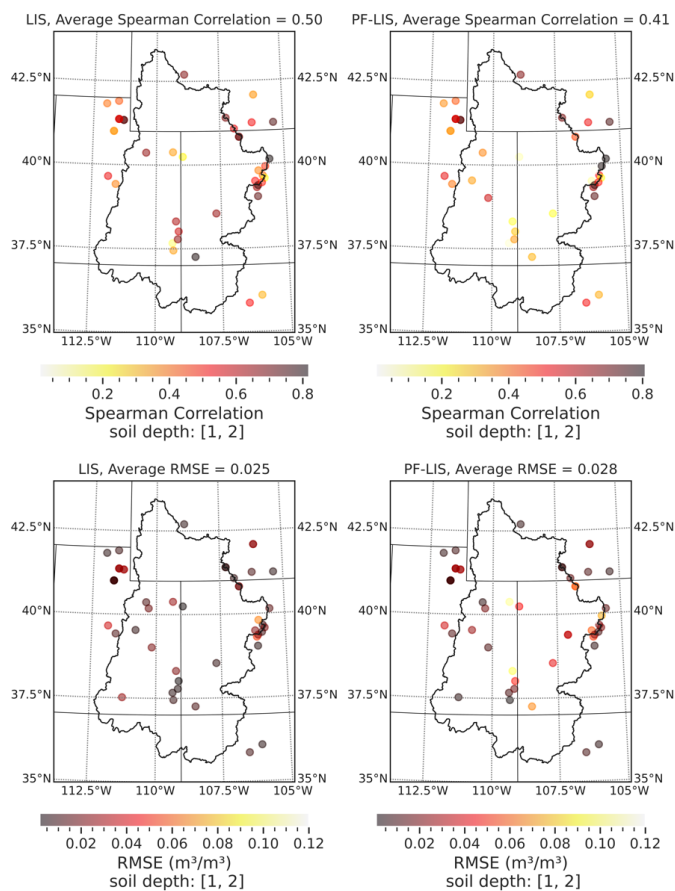
382 LIS/Noah-MP use a form of Richards' equation with some different assumptions. LIS/Noah-MP
383 uses a different function for retention (not the van Genuchten function used within ParFlow) and
384 it is 1D (one-dimensional). The main difference between PF-LIS/Noah-MP and LIS/Noah-MP is
385 the deeper subsurface in PF-LIS/Noah-MP and the fact that it accounts for lateral flow, resulting
386 in a more physically realistic representation of water movement through the soil. This enables the
387 PF-LIS/Noah-MP model to capture the complex influence of topography and specific land surface
388 features on soil moisture.

389 Figure 6 illustrates the comparison between soil moisture estimates from the LIS/Noah-
390 MP and PF-LIS/Noah-MP models against in-situ networks in the UCRB and its adjacent regions.
391 In this section, we focus on presenting the comparison results for the topsoil (Figure 6) and root
392 zone (Figure 7) soil moisture, while the analysis for other soil depths can be found in the
393 supplementary file (Figures S2 and S3). The soil moisture comparison analysis was conducted
394 separately for each soil depth to study the effectiveness and utility of the coupled PF-LIS/Noah-
395 MP model in estimating soil moisture within the coupling soil zone. The 20-year simulation results
396 suggest that, across all four soil depths, the soil moisture values estimated by the PF-LIS/Noah-
397 MP model closely resemble those generated by the LIS/Noah-MP model. The regions' topography
398 (see Figure 2) and the results shown in Figure 5 collectively reveals that the coupled system
399 improves the accuracy of soil moisture estimates across the high altitudes with complex
400 topography in the UCRB. PF-LIS/Noah-MP utilizes the three-dimensional Richards' equation,
401 which is well-suited for accurately modeling soil moisture dynamics in regions with complex
402 topography due to its inherent features and mathematical formulation. The numerical solution of
403 the equation provides flexibility to handle complex boundary conditions in irregular terrains, while
404 its ability to incorporate spatial variability in hydraulic conductivity is vital for representing
405 changing soil properties across challenging landscapes. Moreover, it considers capillary rise and
406 gravitational effects, which are critical factors in areas with elevation changes. These attributes
407 collectively enable the PF-LIS/Noah-MP model to accurately simulate soil moisture dynamics in
408 regions characterized by complex topography. The results confirm that integrating the ParFlow
409 groundwater model with LIS/Noah-MP not only maintains the modeling performance of
410 LIS/Noah-MP but also enhances its ability to represent the spatial variability of land surface
411 processes, as previously demonstrated in Figures 4 and 5.



412
413
414
415
416

Figure 6. The Spearman's correlation coefficient and RMSE between the simulated and observed soil moisture at the soil depth of 0-0.1 m. This result is reported based on 20-year model simulation and observation data, from January 2002 to December 2022.



417
418 *Figure 7. The Spearman's correlation coefficient and RMSE between the simulated and observed*
419 *soil moisture at the soil depth of 1-2 m. This result is reported based on 20-year model*
420 *simulation and observation data, from January 2002 to December 2022.*
421

422 8.2. Streamflow Analysis

423 To calculate the streamflow at the location of the USGS stations, we used ParFlow
424 hydrology module available on ParFlow GitHub page. For more information, we refer the
425 interested readers to this page (<https://github.com/parflow/parflow/tree/master/pftools>). In
426 particular, we used *calculate_overland_flow_grid* that requires different parameters to operate,
427 these include pressure, slopex, slopey, mannings, grid size and the flow method (which is
428 OverlandKinematic here). Figure S4 illustrates the total runoff over the study area for a certain
429 day. We utilized two performance measures, namely Spearman's correlation (Rho) and Total
430 Absolute Relative Bias, to assess the performance of our model on timeseries data. As explained

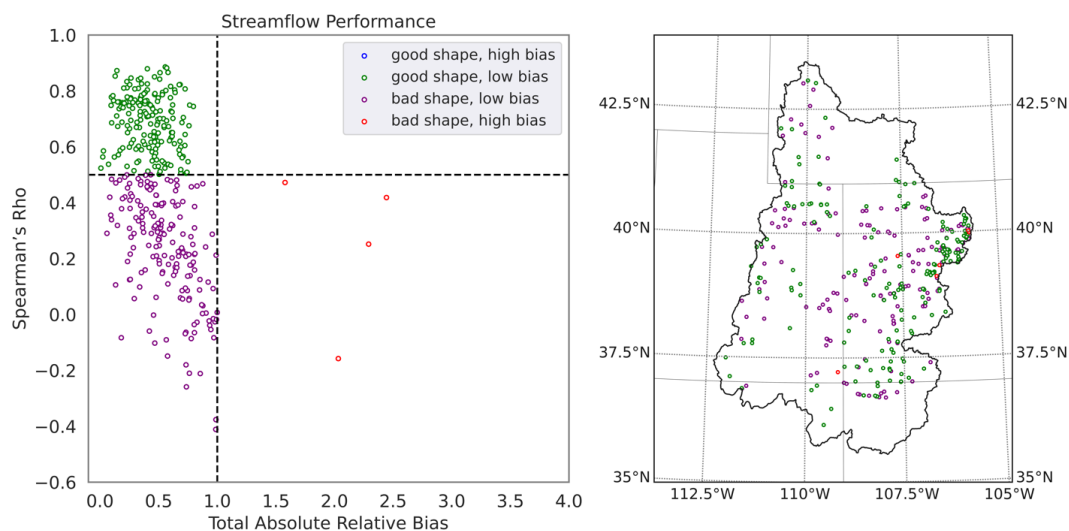


431 in Maxwell and Condon (2016), Tran et al., (2022), O'Neill et al., (2021) and Tijerina-Kreuzer et
432 al., (2021) plotting a graph (hereafter referred to as Condon Diagram) that visualizes these metrics
433 against each other provides a concise representation of the model's capability to accurately
434 simulate the timing and magnitude of streamflow. Spearman's Rho was employed to evaluate
435 disparities in timing between simulated and observed streamflow, while relative bias measured
436 differences in their volumes. A high Spearman's Rho value and a low relative bias value are
437 indications of when simulations closely match observations. If Spearman's Rho is less than 0.5 and
438 Total Absolute Relative Bias is less than 1, the model simulation produces accurate overall flow
439 estimates but does not match the hydrograph peaks well. Conversely, if Spearman's Rho is greater
440 than 0.5 and Total Absolute Relative Bias is less than 1, the model simulation is representing the
441 hydrograph shape (i.e. timing) with low flow bias. However, if Spearman's Rho is less than 0.5
442 and Total Absolute Relative Bias is greater than 1, the model simulation does not reproduce either
443 the flow magnitude or timing. On the other hand, if Spearman's Rho is greater than 0.5 and Total
444 Absolute Relative Bias is greater than 1, the model simulation represents the flow timing well but
445 not the overall flow magnitude. We excluded observations from stations influenced by human
446 activities (Falcone, 2011). While small drainage area basins may experience water withdrawals
447 and irrigation ditches, their susceptibility to anthropogenic influences is significantly lower
448 compared to larger drainage area basins, especially when considering monthly or annual scales
449 (Hao et al., 2008; Zhang et al., 2012). Therefore, we set a drainage area threshold of 500 km², and
450 stations with drainage areas exceeding this threshold underwent manual inspection. For example,
451 we removed the station at Lee's Ferry (drainage area: 289,560 km²), located just downstream of
452 the Glen Canyon Dam, from the analysis.

453 The left panel in Figure 8 shows the Condon Diagram, which summarizes the performance
454 of the PF-LIS/Noah-MP model in estimating streamflow across the USGS stations within the
455 UCRB region. The results indicate that the coupled system has reasonable skill in simulating the
456 streamflow. The right panel in this figure shows the spatial distribution of the USGS stations where
457 the model performance was evaluated. Figure S5 shows the simulated streamflow versus observed
458 streamflow over the period of 20 years at the monitoring location 9066510, which is associated
459 with a stream in Eagle County, Colorado (Spearman's Rho = 0.83 and RMSE=3.65 CMS). Overall,
460 the PF-LIS/Noah-MP model is able to adequately capture the magnitude and timing of streamflow
461 observations. This can be attributed to the robustness of the developed hydrology model, which



462 excels in precisely simulating base flow and its impact on overall streamflow. This lies in the
463 model's comprehensive integration of surface and subsurface hydrological processes. By
464 seamlessly incorporating both surface water and groundwater dynamics, the model achieves a level
465 of accuracy that allows it to effectively simulate streamflow time series, capturing the complex
466 interaction between the surface and subsurface physical processes. The low bias in model
467 simulations also indicates that the model is not systematically overestimating or underestimating
468 streamflow. This further suggests that the model's structure appears to be well-tailored to capture
469 the lateral and vertical water flow and its interaction with the land surface processes.



470
471 *Figure 8. Left panel: The Condon-diagram streamflow performance plot. Right panel: the*
472 *performance category of each gauge within the UCRB domain. This result is reported based on*
473 *20-year model simulation and observation data, from January 2002 to December 2022.*
474

475 8.3. Water Table Depth Analysis

476
477 As mentioned earlier, the most important capability of the PF-LIS/Noah-MP model lies in
478 its ability to estimate groundwater levels up to 392 meters below the land surface. In this study,
479 we employed 10 soil layers with a cumulative depth of 392 meters. However, this depth can be
480 adjusted by the user based on the availability of geological information for the study region. Our
481 comparison of water table depth estimates from the PF-LIS/Noah-MP model with those observed
482 in USGS wells (refer to Table 1) reveals a general agreement between model simulations and
483 observations. However, in some locations the model performance is marginal due to the complex



484 topography of the UCRB. The higher bias observed can likely be attributed to the spatial resolution
 485 of the PF-LIS/Noah-MP model. Deeper wells are typically located in mountainous regions
 486 characterized by complex topography. It is important to note that all wells were assigned to the
 487 nearest grid cell center without any additional adjustments. For example, the USGS station
 488 382427107491401 is associated with a well in Montrose County, Colorado. This well, with a depth
 489 of ~5 meters, is situated in close proximity to agricultural lands and central pivot systems
 490 characterized by a predominantly flat topography. The dataset has been accessible since 2014, and
 491 the reported values for Rho and bias stand at 0.65 and 0.34, respectively. However, at the USGS
 492 station 395136108210000, linked to a well in Rio Blanco County, Colorado, with a depth of ~195
 493 meters, located in a region characterized by more complex terrain and topography, the model's
 494 performance is marginal. Water data has been accessible since 1975. Generally, the model's
 495 performance is contingent upon the geographical locations of the stations. Stations located in
 496 topographically complex surroundings tend to yield lower model performance compared to those
 497 in areas with smoother and flatter environments. Some of the low skill values (reported in Table
 498 1) could be a result of groundwater pumping impacts which are not represented within the
 499 modeling framework.

500 *Table 1: Spearman correlation (Rho) and Total Absolute Relative Bias (TARB)*
 501 *calculated between the water table depth estimated by PF-LIS/Noah-MP and observed by*
 502 *USGS wells.*

Rho	TARB	Latitude	Longitude	USGS Station ID
0.196	0.98	36.490834	-109.94817	362936109564101
-0.79	0.98	36.647222	-110.17068	363850110100801
-0.29	0.81	36.715389	-108.09297	364255108053202
0.62	0.97	36.727221	-110.26319	364338110154601
0.65	0.34	38.4075	-107.82056	382427107491401
0.59	0.08	38.448931	-107.83547	382656107500701
0.63	0.20	38.488056	-107.80861	382917107483101
0.54	0.20	38.496389	-107.78278	382947107465801
0.06	0.48	38.514167	-107.88194	383051107525501
-0.32	0.77	38.554167	-107.88111	383315107525201
-0.28	0.41	38.607222	-107.97083	383626107581501
0.75	0.19	38.685556	-107.985	384110107591801
-0.07	0.47	38.711111	-108.00194	384240108000701
-0.78	0.92	39.86	-108.35111	395136108210000
-0.25	0.94	39.86	-108.35028	395136108210001
-0.63	0.91	39.860133	-108.35096	395136108210004

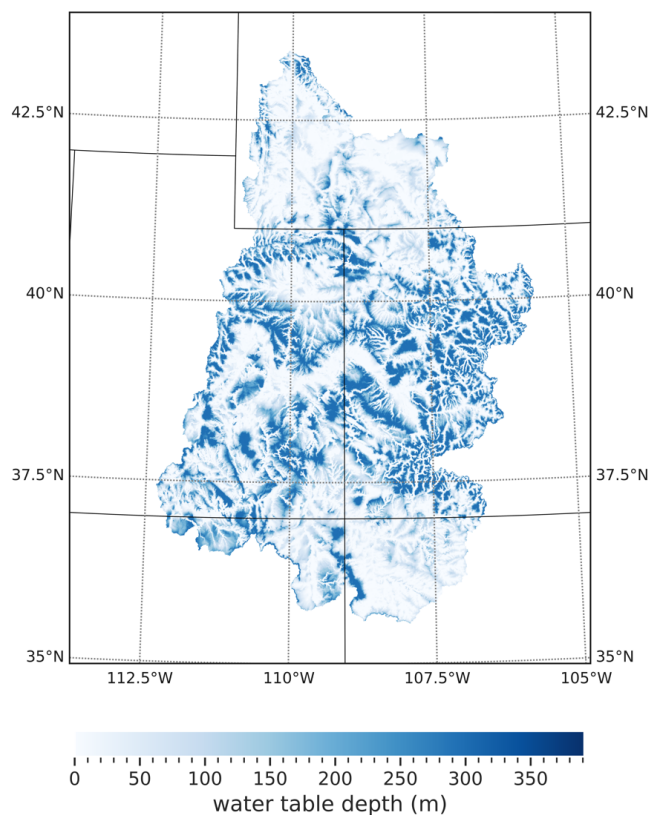


0.98	0.98	39.964444	-108.35417	395755108211400
0.98	0.98	39.964722	-108.35361	395755108211401

503

504 Figure 9, for example, illustrates the water table depth simulated by the PF-LIS/Noah-MP
505 model for a certain day over the UCRB. In general, our observations of water table depth maps
506 over UCRB show more deep water table depth in eastern areas with complex topography, such as
507 hilly or mountainous areas. These areas are often prone to localized variations in the water table.
508 However, regions with smoother topography, like plains, tend to have a more uniform water table
509 pattern, with gradual changes over larger distances. Human activities, such as drainage systems
510 and urbanization, can introduce variability in both types of environments. Overall, water table
511 dynamics are shaped by the interplay of topography, geology, and human influence, with complex
512 topography often contributing to more localized variations compared to smoother environments.

513



514
515
516

Figure 9. Water table depth simulated by PF-LIS/Noah-MP model across the UCRB.

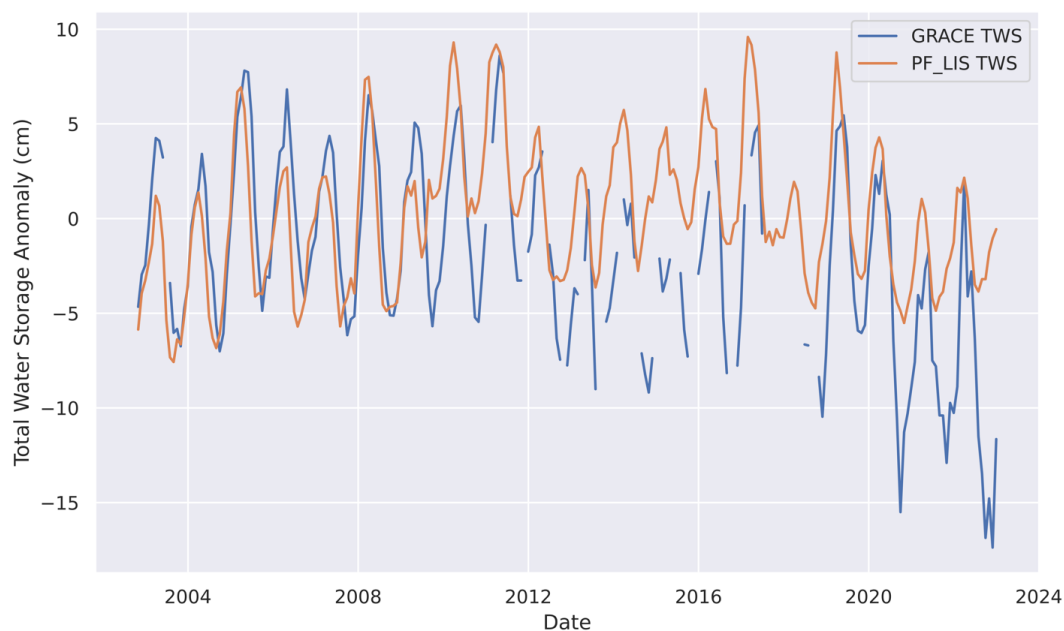


517

518 **8.4. Terrestrial Water Storage Analysis**

519 A comparison between changes in water storage from GRACE and GRACE-FO and the
520 PF-LIS/Noah-MP simulation for the period 2002 to 2022 is shown in Figure 10. The GRACE-
521 derived water storage anomalies were calculated by subtracting the mean water storage from 2004
522 to 2010. The same procedure was applied to the PF-LIS/Noah-MP outputs to maintain consistency
523 in the comparison. The two products demonstrated strong agreement throughout the period from
524 2002 to 2012, effectively capturing the drought years of 2003 and 2004, as well as the wet years
525 of 2005, 2008, and 2011. However, starting from 2013, there is a noticeable decline in the
526 agreement between the two time series, and this disparity becomes more pronounced during the
527 years 2020, 2021, and 2022. The observed disparity is likely attributed to the recent increased
528 anthropogenic effects on groundwater in the UCRB. The increased demand for water, driven by
529 population growth and agricultural expansion, has contributed to a decline in groundwater levels
530 (Carroll et al., 2024; Castle et al., 2014b; Miller et al., 2021; Tillman et al., 2022; Tran et al., 2022).
531 While this trend is accurately captured by the GRACE satellites, PF-LIS/Noah-MP underestimated
532 it. The integration of data assimilation into the coupled system can help to reconcile differences
533 between simulated and observed TWS. LIS already incorporates a data assimilation feature. In our
534 future work, we will study the extent to which the data assimilation capability embedded within
535 LIS improves the representation of the coupled system's response to TWS dynamics.

536



537
538
539
540

Figure 10. Time series of the total water storage anomaly from the PF-LIS/Noah-MP model simulations and the GRACE and GRACE-FO observations.

541 9. Conclusions

542 In this study, we introduced a coupled surface-subsurface hydrology model, PF-LIS/Noah-
543 MP and studied its performance in estimating different hydrologic variables. This study was
544 conducted in the UCRB, a region heavily dependent on groundwater to supply water for millions
545 of people in the western United States. With an anticipated increase in drought occurrences due to
546 climate warming, the region faces a heightened risk of groundwater depletion in the future.
547 Understanding the dynamics of land surface and subsurface water in the UCRB is crucial for
548 effective water resource management and policymaking. In this study, we employed the recently
549 developed integrated surface-subsurface hydrology model, PF-LIS/Noah-MP, to assess key
550 components such as soil moisture, streamflow, water table depth, and total water storage anomaly
551 across the UCRB. These estimations were then compared with a comprehensive set of in-situ and
552 satellite observations, encompassing soil moisture data from various networks, USGS streamflow
553 and well observations, as well as satellite data from SMAP for soil moisture and GRACE for
554 groundwater. The findings demonstrate that the integration of ParFlow with LIS/Noah-MP
555 expands the physics represented by the LIS/Noah-MP model. These increased process



556 representations have two main advantages: better performance of land surface fluxes, especially
557 in regions with complex topography, and accurate estimations of subsurface hydrologic processes,
558 including water table depth. PF-LIS/Noah-MP presents a viable approach to studying land surface
559 and subsurface hydrologic processes and their interactions across different scales. This research
560 contributes valuable insights for informed decision-making in the management of water resources
561 in the UCRB, particularly in the face of future climate challenges. The more detailed representation
562 of subsurface processes within the PF-LIS/Noah-MP system also allows for improved utilization
563 of remote sensing information through data assimilation. For example, to-date, the assimilation of
564 GRACE terrestrial water storage observations has only been demonstrated within models that have
565 a shallow groundwater representation and without the representation of lateral subsurface moisture
566 transport processes (e.g., Kumar et al., 2016). The ongoing development will extend LIS' data
567 assimilation capabilities to PF-LIS, to enable better exploitation of the information from remote
568 sensing.

569 **Competing Interests**

570 At least one of the (co-)authors is a member of the editorial board of Hydrology and Earth
571 System Sciences.

572 **Acknowledgments**

573 Financial support for this project was provided through NASA MAP 80NSSC20K1714.
574 The simulations presented in this article were performed on NASA Discover cluster, provided by
575 the NASA High-End Computing (HEC) Program through the NASA Center for Climate
576 Simulation (NCCS). GRACE and GRACE-FO were jointly developed and operated by NASA,
577 DLR and the GFZ German Research Centre for Geosciences.

578

579 **Authors Contributions**

580 P.A. wrote the first draft of the manuscript. P.A., F.M., C.Y., and D.R. created all the necessary
581 files and datasets for model simulations. P.A. conducted the model simulations and validation
582 analysis. P.A. and R.M. conceptualized the study. R.M., S.K., and M.R. edited the manuscript and
583 helped with the model simulation analysis.



584 **References**

585

586 Alley, W. M.: Another water budget myth: The significance of recoverable ground water in
587 storage, <https://doi.org/10.1111/j.1745-6584.2006.00274.x>, 2007.

588 Arsenault, K. R., Kumar, S. V., Geiger, J. V., Wang, S., Kemp, E., Mocko, D. M., Beaudoin, H.
589 K., Getirana, A., Navari, M., Li, B., Jacob, J., Wegiel, J., and Peters-Lidard, C. D.: The Land
590 surface Data Toolkit (LDT v7.2) - A data fusion environment for land data assimilation systems,
591 *Geosci Model Dev*, 11, <https://doi.org/10.5194/gmd-11-3605-2018>, 2018.

592 Ashby, S. F. and Falgout, R. D.: A parallel multigrid preconditioned conjugate gradient
593 algorithm for groundwater flow simulations, *Nuclear Science and Engineering*, 124,
594 <https://doi.org/10.13182/NSE96-A24230>, 1996.

595 Barthel, R. and Banzhaf, S.: Groundwater and Surface Water Interaction at the Regional-scale –
596 A Review with Focus on Regional Integrated Models, [https://doi.org/10.1007/s11269-015-1163-](https://doi.org/10.1007/s11269-015-1163-z)
597 *z*, 2016.

598 Boucher, O., Myhre, G., and Myhre, A.: Direct human influence of irrigation on atmospheric
599 water vapour and climate, *Clim Dyn*, 22, <https://doi.org/10.1007/s00382-004-0402-4>, 2004.

600 Brookfield, A. E., Ajami, H., Carroll, R. W. H., Tague, C., Sullivan, P. L., and Condon, L. E.:
601 Recent advances in integrated hydrologic models: Integration of new domains,
602 <https://doi.org/10.1016/j.jhydrol.2023.129515>, 1 May 2023.

603 Carroll, R. W. H., Niswonger, R. G., Ulrich, C., Varadharajan, C., Siirila-Woodburn, E. R., and
604 Williams, K. H.: Declining groundwater storage expected to amplify mountain streamflow
605 reductions in a warmer world, *Nature Water*, 2, 419–433, [https://doi.org/10.1038/s44221-024-](https://doi.org/10.1038/s44221-024-00239-0)
606 *00239-0*, 2024.

607 Castle, S. L., Thomas, B. F., Reager, J. T., Rodell, M., Swenson, S. C., and Famiglietti, J. S.:
608 Groundwater depletion during drought threatens future water security of the Colorado River
609 Basin, *Geophys Res Lett*, 41, <https://doi.org/10.1002/2014GL061055>, 2014a.

610 Castle, S. L., Thomas, B. F., Reager, J. T., Rodell, M., Swenson, S. C., and Famiglietti, J. S.:
611 Groundwater depletion during drought threatens future water security of the Colorado River
612 Basin, *Geophys Res Lett*, 41, <https://doi.org/10.1002/2014GL061055>, 2014b.

613 Chan, S. K., Bindlish, R., O'Neill, P. E., Njoku, E., Jackson, T., Colliander, A., Chen, F., Burgin,
614 M., Dunbar, S., Piepmeier, J., Yueh, S., Entekhabi, D., Cosh, M. H., Caldwell, T., Walker, J.,
615 Wu, X., Berg, A., Rowlandson, T., Pacheco, A., McNairn, H., Thibeault, M., Martinez-
616 Fernandez, J., Gonzalez-Zamora, A., Seyfried, M., Bosch, D., Starks, P., Goodrich, D., Prueger,
617 J., Palecki, M., Small, E. E., Zreda, M., Calvet, J. C., Crow, W. T., and Kerr, Y.: Assessment of
618 the SMAP Passive Soil Moisture Product, *IEEE Transactions on Geoscience and Remote*
619 *Sensing*, 54, <https://doi.org/10.1109/TGRS.2016.2561938>, 2016.

620 Christensen, N. S., Wood, A. W., Voisin, N., Lettenmaier, D. P., and Palmer, R. N.: The effects
621 of climate change on the hydrology and water resources of the Colorado River basin, *Clim*
622 *Change*, 62, <https://doi.org/10.1023/B:CLIM.0000013684.13621.1f>, 2004.

623 Condon, L. E. and Maxwell, R. M.: Modified priority flood and global slope enforcement
624 algorithm for topographic processing in physically based hydrologic modeling applications,
625 *Comput Geosci*, 126, <https://doi.org/10.1016/j.cageo.2019.01.020>, 2019.



- 626 Cook, B. I., Ault, T. R., and Smerdon, J. E.: Unprecedented 21st century drought risk in the
627 American Southwest and Central Plains, <https://doi.org/10.1126/sciadv.1400082>, 2015.
- 628 Cook, B. I., Mankin, J. S., Williams, A. P., Marvel, K. D., Smerdon, J. E., and Liu, H.:
629 Uncertainties, Limits, and Benefits of Climate Change Mitigation for Soil Moisture Drought in
630 Southwestern North America, *Earths Future*, 9, <https://doi.org/10.1029/2021EF002014>, 2021.
- 631 Crow, W. T., Kumar, S. V., and Bolten, J. D.: On the utility of land surface models for
632 agricultural drought monitoring, *Hydrol Earth Syst Sci*, 16, <https://doi.org/10.5194/hess-16-3451-2012>, 2012.
- 634 Deb, P., Kiem, A. S., and Willgoose, G.: A linked surface water-groundwater modelling
635 approach to more realistically simulate rainfall-runoff non-stationarity in semi-arid regions, *J*
636 *Hydrol (Amst)*, 575, <https://doi.org/10.1016/j.jhydrol.2019.05.039>, 2019.
- 637 Döll, P., Hoffmann-Dobrev, H., Portmann, F. T., Siebert, S., Eicker, A., Rodell, M., Strassberg,
638 G., and Scanlon, B. R.: Impact of water withdrawals from groundwater and surface water on
639 continental water storage variations, *J Geodyn*, 59–60, <https://doi.org/10.1016/j.jog.2011.05.001>,
640 2012.
- 641 Falcone, J. A.: GAGES-II: Geospatial Attributes of Gages for Evaluating Streamflow (Digital
642 Dataset), 2011.
- 643 Famiglietti, J. S., Lo, M., Ho, S. L., Bethune, J., Anderson, K. J., Syed, T. H., Swenson, S. C.,
644 De Linage, C. R., and Rodell, M.: Satellites measure recent rates of groundwater depletion in
645 California’s Central Valley, *Geophys Res Lett*, 38, <https://doi.org/10.1029/2010GL046442>,
646 2011.
- 647 Famiglietti, J. S., Rodell, M., Durack, P. J., Trenberth, K. E., Held, I. M., Soden, B. J., Tiwari, V.
648 M., Wahr, J., Swenson, S., Scanlon, B. R., Voss, K. A., Tapley, B. D., Reager, J. T., Famiglietti,
649 J. S., Houborg, R., Blunden, J., Arndt, D. S., Zaitchik, B. F., Swenson, S. C., Milly, P. C. D.,
650 Ramillien, G., Swenson, S., Wahr, J., and Famiglietti, J. S.: Environmental science. Water in the
651 balance., *Science*, 340, 2013.
- 652 Fan, Y., Miguez-Macho, G., Weaver, C. P., Walko, R., and Robock, A.: Incorporating water
653 table dynamics in climate modeling: 1. Water table observations and equilibrium water table
654 simulations, *Journal of Geophysical Research Atmospheres*, 112,
655 <https://doi.org/10.1029/2006JD008111>, 2007.
- 656 Fan, Y., Li, H., and Miguez-Macho, G.: Global patterns of groundwater table depth, *Science*
657 (1979), 339, <https://doi.org/10.1126/science.1229881>, 2013.
- 658 Fleckenstein, J. H., Krause, S., Hannah, D. M., and Boano, F.: Groundwater-surface water
659 interactions: New methods and models to improve understanding of processes and dynamics,
660 *Adv Water Resour*, 33, <https://doi.org/10.1016/j.advwatres.2010.09.011>, 2010.
- 661 Getirana, A., Jung, H. C., Arsenault, K., Shukla, S., Kumar, S., Peters-Lidard, C., Maigari, I.,
662 and Mamane, B.: Satellite Gravimetry Improves Seasonal Streamflow Forecast Initialization in
663 Africa, *Water Resour Res*, 56, <https://doi.org/10.1029/2019WR026259>, 2020.
- 664 Gordon, L. J., Steffen, W., Jönsson, B. F., Folke, C., Falkenmark, M., and Johannessen, Å.:
665 Human modification of global water vapor flows from the land surface, *Proc Natl Acad Sci U S*
666 *A*, 102, <https://doi.org/10.1073/pnas.0500208102>, 2005.



- 667 Green, T. R., Taniguchi, M., Kooi, H., Gurdak, J. J., Allen, D. M., Hiscock, K. M., Treidel, H.,
668 and Aureli, A.: Beneath the surface of global change: Impacts of climate change on groundwater,
669 <https://doi.org/10.1016/j.jhydrol.2011.05.002>, 2011.
- 670 Hao, X., Chen, Y., Xu, C., and Li, W.: Impacts of climate change and human activities on the
671 surface runoff in the Tarim River Basin over the last fifty years, *Water Resources Management*,
672 22, <https://doi.org/10.1007/s11269-007-9218-4>, 2008.
- 673 Harding, K. J. and Snyder, P. K.: Modeling the atmospheric response to irrigation in the great
674 plains. Part I: General impacts on precipitation and the energy budget, *J Hydrometeorol*, 13,
675 <https://doi.org/10.1175/JHM-D-11-098.1>, 2012.
- 676 Hutson, S. S., Barber, N. L., Kenny, J. F., Linsey, K. S., Lumia, D. S., and Maupin, M. A.:
677 Estimated use of water in the United States in 2000, US Geological Survey Circular, 2004.
- 678 Jasechko, S., Perrone, D., Befus, K. M., Bayani Cardenas, M., Ferguson, G., Gleeson, T.,
679 Luijendijk, E., McDonnell, J. J., Taylor, R. G., Wada, Y., and Kirchner, J. W.: Global aquifers
680 dominated by fossil groundwaters but wells vulnerable to modern contamination, *Nat Geosci*, 10,
681 <https://doi.org/10.1038/ngeo2943>, 2017.
- 682 Jones, J. E. and Woodward, C. S.: Newton-Krylov-multigrid solvers for large-scale, highly
683 heterogeneous, variably saturated flow problems, *Adv Water Resour*, 24,
684 [https://doi.org/10.1016/S0309-1708\(00\)00075-0](https://doi.org/10.1016/S0309-1708(00)00075-0), 2001.
- 685 Kalbus, E., Reinstorf, F., and Schirmer, M.: Measuring methods for groundwater - Surface water
686 interactions: A review, <https://doi.org/10.5194/hess-10-873-2006>, 2006.
- 687 Kawase, H., Yoshikane, T., Hara, M., Kimura, F., Sato, T., and Ohsawa, S.: Impact of extensive
688 irrigation on the formation of cumulus clouds, *Geophys Res Lett*, 35,
689 <https://doi.org/10.1029/2007GL032435>, 2008.
- 690 Kenny, J. F., Barber, N. L., Hutson, S. S., Linsey, K. S., Lovelace, J. K., and Maupin, M. A.:
691 Estimated Use of Water in the United States in 2005 Circular 1344, Water, 2005.
- 692 Kollet, S. J. and Maxwell, R. M.: Integrated surface-groundwater flow modeling: A free-surface
693 overland flow boundary condition in a parallel groundwater flow model, *Adv Water Resour*, 29,
694 <https://doi.org/10.1016/j.advwatres.2005.08.006>, 2006.
- 695 Kollet, S. J. and Maxwell, R. M.: Capturing the influence of groundwater dynamics on land
696 surface processes using an integrated, distributed watershed model, *Water Resour Res*, 44,
697 <https://doi.org/10.1029/2007WR006004>, 2008.
- 698 Kollet, S. J., Maxwell, R. M., Woodward, C. S., Smith, S., Vanderborght, J., Vereecken, H., and
699 Simmer, C.: Proof of concept of regional scale hydrologic simulations at hydrologic resolution
700 utilizing massively parallel computer resources, *Water Resour Res*, 46,
701 <https://doi.org/10.1029/2009WR008730>, 2010.
- 702 Kourakos, G., Dahlke, H. E., and Harter, T.: Increasing Groundwater Availability and Seasonal
703 Base Flow Through Agricultural Managed Aquifer Recharge in an Irrigated Basin, *Water Resour*
704 *Res*, 55, <https://doi.org/10.1029/2018WR024019>, 2019.
- 705 Krakauer, N. Y., Li, H., and Fan, Y.: Groundwater flow across spatial scales: Importance for
706 climate modeling, *Environmental Research Letters*, 9, [https://doi.org/10.1088/1748-](https://doi.org/10.1088/1748-9326/9/3/034003)
707 [9326/9/3/034003](https://doi.org/10.1088/1748-9326/9/3/034003), 2014.



- 708 Kuffour, B. N. O., Engdahl, N. B., Woodward, C. S., Condon, L. E., Kollet, S., and Maxwell, R.
709 M.: Simulating coupled surface-subsurface flows with ParFlow v3.5.0: Capabilities, applications,
710 and ongoing development of an open-source, massively parallel, integrated hydrologic model,
711 *Geosci Model Dev*, 13, <https://doi.org/10.5194/gmd-13-1373-2020>, 2020.
- 712 Kumar, S. V., Peters-Lidard, C. D., Tian, Y., Houser, P. R., Geiger, J., Olden, S., Lighty, L.,
713 Eastman, J. L., Doty, B., Dirmeyer, P., Adams, J., Mitchell, K., Wood, E. F., and Sheffield, J.:
714 Land information system: An interoperable framework for high resolution land surface
715 modeling, *Environmental Modelling and Software*, 21, 1402–1415,
716 <https://doi.org/10.1016/j.envsoft.2005.07.004>, 2006.
- 717 Kumar, S. V., Reichle, R. H., Peters-Lidard, C. D., Koster, R. D., Zhan, X., Crow, W. T.,
718 Eylander, J. B., and Houser, P. R.: A land surface data assimilation framework using the land
719 information system: Description and applications, *Adv Water Resour*, 31,
720 <https://doi.org/10.1016/j.advwatres.2008.01.013>, 2008a.
- 721 Kumar, S. V., Reichle, R. H., Peters-Lidard, C. D., Koster, R. D., Zhan, X., Crow, W. T.,
722 Eylander, J. B., and Houser, P. R.: A land surface data assimilation framework using the land
723 information system: Description and applications, *Adv Water Resour*, 31,
724 <https://doi.org/10.1016/j.advwatres.2008.01.013>, 2008b.
- 725 Kumar, S. V., Peters-Lidard, C. D., Eastman, J. L., and Tao, W. K.: An integrated high-
726 resolution hydrometeorological modeling testbed using LIS and WRF, *Environmental Modelling*
727 *and Software*, 23, <https://doi.org/10.1016/j.envsoft.2007.05.012>, 2008c.
- 728 Kumar, S. V., Zaitchik, B. F., Peters-Lidard, C. D., Rodell, M., Reichle, R., Li, B., Jasinski, M.,
729 Mocko, D., Getirana, A., De Lannoy, G., Cosh, M. H., Hain, C. R., Anderson, M., Arsenault, K.
730 R., Xia, Y., and Ek, M.: Assimilation of Gridded GRACE terrestrial water storage estimates in
731 the North American land data assimilation system, *J Hydrometeorol*, 17,
732 <https://doi.org/10.1175/JHM-D-15-0157.1>, 2016.
- 733 Lahmers, T. M., Kumar, S. V., Rosen, D., Dugger, A., Gochis, D. J., Santanello, J. A.,
734 Gangodagamage, C., and Dunlap, R.: Assimilation of NASA's Airborne Snow Observatory
735 Snow Measurements for Improved Hydrological Modeling: A Case Study Enabled by the
736 Coupled LIS/WRF-Hydro System, *Water Resour Res*, 58,
737 <https://doi.org/10.1029/2021WR029867>, 2022.
- 738 Landerer, F. W., Flechtner, F. M., Save, H., Webb, F. H., Bandikova, T., Bertiger, W. I.,
739 Bettadpur, S. V., Byun, S. H., Dahle, C., Dobslaw, H., Fahnestock, E., Harvey, N., Kang, Z.,
740 Kruizinga, G. L. H., Loomis, B. D., McCullough, C., Murböck, M., Nagel, P., Paik, M., Pie, N.,
741 Poole, S., Strelakov, D., Tamisiea, M. E., Wang, F., Watkins, M. M., Wen, H. Y., Wiese, D. N.,
742 and Yuan, D. N.: Extending the Global Mass Change Data Record: GRACE Follow-On
743 Instrument and Science Data Performance, *Geophys Res Lett*, 47,
744 <https://doi.org/10.1029/2020GL088306>, 2020.
- 745 Leng, G., Huang, M., Tang, Q., Gao, H., and Leung, L. R.: Modeling the effects of groundwater-
746 fed irrigation on terrestrial hydrology over the conterminous United States, *J Hydrometeorol*, 15,
747 <https://doi.org/10.1175/JHM-D-13-049.1>, 2014.
- 748 Leung, L. R., Huang, M., Qian, Y., and Liang, X.: Climate-soil-vegetation control on
749 groundwater table dynamics and its feedbacks in a climate model, *Clim Dyn*, 36,
750 <https://doi.org/10.1007/s00382-010-0746-x>, 2011.



- 751 Li, B., Rodell, M., Kumar, S., Beaudoin, H. K., Getirana, A., Zaitchik, B. F., de Goncalves, L.
752 G., Cossetin, C., Bhanja, S., Mukherjee, A., Tian, S., Tangdamrongsub, N., Long, D., Nanteza,
753 J., Lee, J., Policelli, F., Goni, I. B., Daira, D., Bila, M., de Lannoy, G., Mocko, D., Steele-Dunne,
754 S. C., Save, H., and Bettadpur, S.: Global GRACE Data Assimilation for Groundwater and
755 Drought Monitoring: Advances and Challenges, *Water Resour Res*, 55,
756 <https://doi.org/10.1029/2018WR024618>, 2019.
- 757 Li, B., Rodell, M., Peters-Lidard, C., Erlingis, J., Kumar, S., and Mocko, D.: Groundwater
758 recharge estimated by land surface models: An evaluation in the conterminous United States, *J*
759 *Hydrometeorol*, 22, <https://doi.org/10.1175/JHM-D-20-0130.1>, 2021.
- 760 Liang, X., Xie, Z., and Huang, M.: A new parameterization for surface and groundwater
761 interactions and its impact on water budgets with the variable infiltration capacity (VIC) land
762 surface model, *Journal of Geophysical Research: Atmospheres*, 108,
763 <https://doi.org/10.1029/2002jd003090>, 2003.
- 764 Liu, P. W., Bindlish, R., Oaneill, P., Fang, B., Lakshmi, V., Yang, Z., Cosh, M. H., Bongiovanni,
765 T., Collins, C. H., Starks, P. J., Prueger, J., Bosch, D. D., Seyfried, M., and Williams, M. R.:
766 Thermal Hydraulic Disaggregation of SMAP Soil Moisture Over the Continental United States,
767 *IEEE J Sel Top Appl Earth Obs Remote Sens*, 15,
768 <https://doi.org/10.1109/JSTARS.2022.3165644>, 2022.
- 769 Liu, Y., Peters-Lidard, C. D., Kumar, S. V., Arsenault, K. R., and Mocko, D. M.: Blending
770 satellite-based snow depth products with in situ observations for streamflow predictions in the
771 Upper Colorado River Basin, *Water Resour Res*, 51, <https://doi.org/10.1002/2014WR016606>,
772 2015.
- 773 Lo, M. H. and Famiglietti, J. S.: Irrigation in California's Central Valley strengthens the
774 southwestern U.S. water cycle, *Geophys Res Lett*, 40, <https://doi.org/10.1002/grl.50108>, 2013.
- 775 Maurer, E. P., Wood, A. W., Adam, J. C., Lettenmaier, D. P., and Nijssen, B.: A Long-Term
776 Hydrologically Based Dataset of Land Surface Fluxes and States for the Conterminous United
777 States *, n.d.
- 778 Maxwell, R. M.: A terrain-following grid transform and preconditioner for parallel, large-scale,
779 integrated hydrologic modeling, *Adv Water Resour*, 53,
780 <https://doi.org/10.1016/j.advwatres.2012.10.001>, 2013.
- 781 Maxwell, R. M. and Condon, L. E.: Connections between groundwater flow and transpiration
782 partitioning, *Science* (1979), 353, <https://doi.org/10.1126/science.aaf7891>, 2016.
- 783 Maxwell, R. M., Chow, F. K., and Kollet, S. J.: The groundwater-land-surface-atmosphere
784 connection: Soil moisture effects on the atmospheric boundary layer in fully-coupled
785 simulations, *Adv Water Resour*, 30, <https://doi.org/10.1016/j.advwatres.2007.05.018>, 2007.
- 786 Maxwell, R. M., Lundquist, J. K., Mirocha, J. D., Smith, S. G., Woodward, C. S., and Tompson,
787 A. F. B.: Development of a coupled groundwater-atmosphere model, *Mon Weather Rev*, 139,
788 <https://doi.org/10.1175/2010MWR3392.1>, 2011.
- 789 Maxwell, R. M., Putti, M., Meyerhoff, S., Delfs, J. O., Ferguson, I. M., Ivanov, V., Kim, J.,
790 Kolditz, O., Kollet, S. J., Kumar, M., Lopez, S., Niu, J., Paniconi, C., Park, Y. J., Phanikumar,
791 M. S., Shen, C., Sudicky, E. A., and Sulis, M.: Surface-subsurface model intercomparison: A



- 792 first set of benchmark results to diagnose integrated hydrology and feedbacks, *Water Resour*
793 *Res*, 50, <https://doi.org/10.1002/2013WR013725>, 2014a.
- 794 Maxwell, R. M., Putti, M., Meyerhoff, S., Delfs, J. O., Ferguson, I. M., Ivanov, V., Kim, J.,
795 Kolditz, O., Kollet, S. J., Kumar, M., Lopez, S., Niu, J., Paniconi, C., Park, Y. J., Phanikumar,
796 M. S., Shen, C., Sudicky, E. A., and Sulis, M.: Surface-subsurface model intercomparison: A
797 first set of benchmark results to diagnose integrated hydrology and feedbacks, *Water Resour*
798 *Res*, 50, <https://doi.org/10.1002/2013WR013725>, 2014b.
- 799 Maxwell, R. M., Condon, L. E., and Kollet, S. J.: A high-resolution simulation of groundwater
800 and surface water over most of the continental US with the integrated hydrologic model ParFlow
801 v3, *Geosci Model Dev*, 8, <https://doi.org/10.5194/gmd-8-923-2015>, 2015.
- 802 Miguez-Macho, G., Fan, Y., Weaver, C. P., Walko, R., and Robock, A.: Incorporating water
803 table dynamics in climate modeling: 2. Formulation, validation, and soil moisture simulation,
804 *Journal of Geophysical Research Atmospheres*, 112, <https://doi.org/10.1029/2006JD008112>,
805 2007.
- 806 Miller, M. P., Buto, S. G., Susong, D. D., and Rumsey, C. A.: The importance of base flow in
807 sustaining surface water flow in the Upper Colorado River Basin, *Water Resour Res*, 52,
808 <https://doi.org/10.1002/2015WR017963>, 2016.
- 809 Miller, O. L., Miller, M. P., Longley, P. C., Alder, J. R., Bearup, L. A., Pruitt, T., Jones, D. K.,
810 Putman, A. L., Rumsey, C. A., and McKinney, T.: How Will Baseflow Respond to Climate
811 Change in the Upper Colorado River Basin?, *Geophys Res Lett*, 48,
812 <https://doi.org/10.1029/2021GL095085>, 2021.
- 813 Mocko, D. M., Kumar, S. V., Peters-Lidard, C. D., and Wang, S.: Assimilation of vegetation
814 conditions improves the representation of drought over agricultural areas, *J Hydrometeorol*, 22,
815 <https://doi.org/10.1175/JHM-D-20-0065.1>, 2021.
- 816 Naz, B. S., Sharples, W., Ma, Y., Goergen, K., and Kollet, S.: Continental-scale evaluation of a
817 fully distributed coupled land surface and groundwater model, ParFlow-CLM (v3.6.0), over
818 Europe, *Geosci Model Dev*, 16, 1617–1639, <https://doi.org/10.5194/gmd-16-1617-2023>, 2023.
- 819 Nie, W., Kumar, S. V., Arsenault, K. R., Peters-Lidard, C. D., Mladenova, I. E., Bergaoui, K.,
820 Hazra, A., Zaitchik, B. F., Mahanama, S. P., McDonnell, R., Mocko, D. M., and Navari, M.:
821 Towards effective drought monitoring in the Middle East and North Africa (MENA) region:
822 implications from assimilating leaf area index and soil moisture into the Noah-MP land surface
823 model for Morocco, *Hydrol Earth Syst Sci*, 26, <https://doi.org/10.5194/hess-26-2365-2022>, 2022.
- 824 Niu, G. Y., Yang, Z. L., Mitchell, K. E., Chen, F., Ek, M. B., Barlage, M., Kumar, A., Manning,
825 K., Niyogi, D., Rosero, E., Tewari, M., and Xia, Y.: The community Noah land surface model
826 with multiparameterization options (Noah-MP): 1. Model description and evaluation with local-
827 scale measurements, *Journal of Geophysical Research Atmospheres*, 116,
828 <https://doi.org/10.1029/2010JD015139>, 2011.
- 829 Ntona, M. M., Busico, G., Mastrocicco, M., and Kazakis, N.: Modeling groundwater and surface
830 water interaction: An overview of current status and future challenges,
831 <https://doi.org/10.1016/j.scitotenv.2022.157355>, 2022.
- 832 Oki, T. and Kanae, S.: Global hydrological cycles and world water resources,
833 <https://doi.org/10.1126/science.1128845>, 2006.



- 834 O’neill, M. M. F., Tijerina, D. T., Condon, L. E., and Maxwell, R. M.: Assessment of the
835 ParFlow-CLM CONUS 1.0 integrated hydrologic model: evaluation of hyper-resolution water
836 balance components across the contiguous United States, *Geosci Model Dev*, 14,
837 <https://doi.org/10.5194/gmd-14-7223-2021>, 2021a.
- 838 O’neill, M. M. F., Tijerina, D. T., Condon, L. E., and Maxwell, R. M.: Assessment of the
839 ParFlow-CLM CONUS 1.0 integrated hydrologic model: evaluation of hyper-resolution water
840 balance components across the contiguous United States, *Geosci Model Dev*, 14,
841 <https://doi.org/10.5194/gmd-14-7223-2021>, 2021b.
- 842 Painter, T. H., Skiles, S. M. K., Deems, J. S., Bryant, A. C., and Landry, C. C.: Dust radiative
843 forcing in snow of the Upper Colorado River Basin: 1. A 6 year record of energy balance,
844 radiation, and dust concentrations, *Water Resour Res*, 48,
845 <https://doi.org/10.1029/2012WR011985>, 2012.
- 846 Peters-Lidard, C. D., Houser, P. R., Tian, Y., Kumar, S. V., Geiger, J., Olden, S., Lighty, L.,
847 Doty, B., Dirmeyer, P., Adams, J., Mitchell, K., Wood, E. F., and Sheffield, J.: High-
848 performance Earth system modeling with NASA/GSFC’s Land Information System, *Innov Syst*
849 *Softw Eng*, 3, <https://doi.org/10.1007/s11334-007-0028-x>, 2007.
- 850 Qian, Y., Huang, M., Yang, B., and Berg, L. K.: A modeling study of irrigation effects on
851 surface fluxes and land-air-cloud interactions in the southern great plains, *J Hydrometeorol*, 14,
852 <https://doi.org/10.1175/JHM-D-12-0134.1>, 2013.
- 853 Rodell, M. and Reager, J. T.: Water cycle science enabled by the GRACE and GRACE-FO
854 satellite missions, *Nature Water*, 1, <https://doi.org/10.1038/s44221-022-00005-0>, 2023.
- 855 Sacks, W. J., Cook, B. I., Buening, N., Levis, S., and Helkowski, J. H.: Effects of global
856 irrigation on the near-surface climate, *Clim Dyn*, 33, <https://doi.org/10.1007/s00382-008-0445-z>,
857 2009.
- 858 Save, H., Bettadpur, S., and Tapley, B. D.: High-resolution CSR GRACE RL05 mascons, *J*
859 *Geophys Res Solid Earth*, 121, <https://doi.org/10.1002/2016JB013007>, 2016.
- 860 Scanlon, B. R., Faunt, C. C., Longuevergne, L., Reedy, R. C., Alley, W. M., McGuire, V. L., and
861 McMahon, P. B.: Groundwater depletion and sustainability of irrigation in the US High Plains
862 and Central Valley, *Proc Natl Acad Sci U S A*, 109, <https://doi.org/10.1073/pnas.1200311109>,
863 2012.
- 864 Scanlon, B. R., Zhang, Z., Save, H., Wiese, D. N., Landerer, F. W., Long, D., Longuevergne, L.,
865 and Chen, J.: Global evaluation of new GRACE mascon products for hydrologic applications,
866 *Water Resour Res*, 52, <https://doi.org/10.1002/2016WR019494>, 2016.
- 867 Tang, Q., Oki, T., Kanae, S., and Hu, H.: The influence of precipitation variability and partial
868 irrigation within grid cells on a hydrological simulation, *J Hydrometeorol*, 8,
869 <https://doi.org/10.1175/JHM589.1>, 2007.
- 870 Tapley, B. D., Bettadpur, S., Watkins, M., and Reigber, C.: The gravity recovery and climate
871 experiment: Mission overview and early results, *Geophys Res Lett*, 31,
872 <https://doi.org/10.1029/2004GL019920>, 2004.
- 873 Taylor, R. G., Scanlon, B., Döll, P., Rodell, M., Van Beek, R., Wada, Y., Longuevergne, L.,
874 Leblanc, M., Famiglietti, J. S., Edmunds, M., Konikow, L., Green, T. R., Chen, J., Taniguchi,



- 875 M., Bierkens, M. F. P., Macdonald, A., Fan, Y., Maxwell, R. M., Yechieli, Y., Gurdak, J. J.,
876 Allen, D. M., Shamsudduha, M., Hiscock, K., Yeh, P. J. F., Holman, I., and Treidel, H.: Ground
877 water and climate change, <https://doi.org/10.1038/nclimate1744>, 2013.
- 878 Supplemental Environmental Impact Statement for Near-term Colorado River Operations:
879 Tian, Y., Zheng, Y., Wu, B., Wu, X., Liu, J., and Zheng, C.: Modeling surface water-
880 groundwater interaction in arid and semi-arid regions with intensive agriculture, *Environmental*
881 *Modelling and Software*, 63, <https://doi.org/10.1016/j.envsoft.2014.10.011>, 2015.
- 882 Tijerina, D., Condon, L., FitzGerald, K., Dugger, A., O'Neill, M. M., Sampson, K., Gochis, D.,
883 and Maxwell, R.: Continental Hydrologic Intercomparison Project, Phase 1: A Large-Scale
884 Hydrologic Model Comparison Over the Continental United States, *Water Resour Res*, 57,
885 <https://doi.org/10.1029/2020WR028931>, 2021.
- 886 Tijerina-Kreuzer, D., Swilley, J. S., Tran, H. V., Zhang, J., West, B., Yang, C., Condon, L. E.,
887 and Maxwell, R. M.: Continental Scale Hydrostratigraphy: Basin-Scale Testing of Alternative
888 Data-Driven Approaches, *Groundwater*, 62, <https://doi.org/10.1111/gwat.13357>, 2024.
- 889 Tillman, F. D., Day, N. K., Miller, M. P., Miller, O. L., Rumsey, C. A., Wise, D. R., Longley, P.
890 C., and McDonnell, M. C.: A Review of Current Capabilities and Science Gaps in Water Supply
891 Data, Modeling, and Trends for Water Availability Assessments in the Upper Colorado River
892 Basin, <https://doi.org/10.3390/w14233813>, 2022.
- 893 Tran, H., Zhang, J., O'Neill, M. M., Ryken, A., Condon, L. E., and Maxwell, R. M.: A
894 hydrological simulation dataset of the Upper Colorado River Basin from 1983 to 2019, *Sci Data*,
895 9, <https://doi.org/10.1038/s41597-022-01123-w>, 2022.
- 896 U.S. Department of the Interior: Colorado River Basin SECURE Water Act Section 9503(c)
897 Report to Congress, 2021.
- 898 Wada, Y., Van Beek, L. P. H., Van Kempen, C. M., Reckman, J. W. T. M., Vasak, S., and
899 Bierkens, M. F. P.: Global depletion of groundwater resources, *Geophys Res Lett*, 37,
900 <https://doi.org/10.1029/2010GL044571>, 2010.
- 901 Wang, Y. and Chen, N.: Recent progress in coupled surface-ground water models and their
902 potential in watershed hydro-biogeochemical studies: A review, *Watershed Ecology and the*
903 *Environment*, 3, <https://doi.org/10.1016/j.wsee.2021.04.001>, 2021.
- 904 Williams, A. P., Cook, B. I., and Smerdon, J. E.: Rapid intensification of the emerging
905 southwestern North American megadrought in 2020–2021, *Nat Clim Chang*, 12,
906 <https://doi.org/10.1038/s41558-022-01290-z>, 2022.
- 907 Winter, T. C., Harvey, J. W., Franke, O. L., and Alley, W. M.: Ground Water and Surface Water
908 - A single Resource - U.S. Geological Survey Circular 1139, USGS Publications, Circular 1,
909 1998.
- 910 Xia, Y., Mitchell, K., Ek, M., Cosgrove, B., Sheffield, J., Luo, L., Alonge, C., Wei, H., Meng, J.,
911 Livneh, B., Duan, Q., and Lohmann, D.: Continental-scale water and energy flux analysis and
912 validation for North American Land Data Assimilation System project phase 2 (NLDAS-2): 2.
913 Validation of model-simulated streamflow, *Journal of Geophysical Research Atmospheres*, 117,
914 <https://doi.org/10.1029/2011JD016051>, 2012.



- 915 Yang, C., Tijerina-Kreuzer, D. T., Tran, H. V., Condon, L. E., and Maxwell, R. M.: A high-
916 resolution, 3D groundwater-surface water simulation of the contiguous US: Advances in the
917 integrated ParFlow CONUS 2.0 modeling platform, *J Hydrol (Amst)*, 626,
918 <https://doi.org/10.1016/j.jhydrol.2023.130294>, 2023.
- 919 Yang, X., Hu, J., Ma, R., and Sun, Z.: Integrated Hydrologic Modelling of Groundwater-Surface
920 Water Interactions in Cold Regions, <https://doi.org/10.3389/feart.2021.721009>, 1 December
921 2021.
- 922 Zhang, A., Zhang, C., Fu, G., Wang, B., Bao, Z., and Zheng, H.: Assessments of Impacts of
923 Climate Change and Human Activities on Runoff with SWAT for the Huifa River Basin,
924 Northeast China, *Water Resources Management*, 26, <https://doi.org/10.1007/s11269-012-0010-8>,
925 2012.
- 926 Zhang, J., Condon, L. E., Tran, H., and Maxwell, R. M.: A national topographic dataset for
927 hydrological modeling over the contiguous United States, *Earth Syst Sci Data*, 13,
928 <https://doi.org/10.5194/essd-13-3263-2021>, 2021.